THE JOURNAL OF PHYSICAL CHEMISTRY LETTERS
A JOURNAL OF THE AMERICAN CHEMICAL SOCIETY

Open Access
This article is licensed under CC-BY-NC-ND 4.0

pubs.acs.org/JPCL
Letter

Temperature-Enhanced Coercive Field by Chiral Molecules

Yael Kapon,[‖] Lilach Brann,[‖] Shira Yochelis, Jonas Fransson, Dimitar D. Sasselov, Yossi Paltiel, and S. Furkan Ozturk*

Cite This: J. Phys. Chem. Lett. 2026, 17, 5115−5121
Read Online

ACCESS | Metrics & More | Article Recommendations | Supporting Information

ABSTRACT: The chiral-induced spin selectivity (CISS) effect demonstrates a strong coupling between electron spin and molecular chirality, enabling spin-controlled interactions between chiral molecules and magnetic surfaces. While CISS experiments have revealed robust changes in the spin-polarization properties of magnetic materials upon chiral molecular adsorption, the temperature dependence of these effects remains poorly understood. Here, we investigate the temperature dependence of the chirality-induced increase in magnetic coercivity by ribose-aminooxazoline (RAO) crystals on ferromagnetic surfaces. RAO was selected as a conglomerate-forming, thermodynamically stable crystalline chiral organic molecule with prebiotic relevance that has previously been shown to induce strong spin-dependent changes in magnetic minerals. Contrary to classical expectations that magnetic coercivity weakens at elevated temperatures, we observe a significant increase in magnetic coercivity (∼1 mT over a 60 °C temperature change) with increasing temperature. These results support a vibronic contribution to CISS arising from electron−phonon interactions and demonstrate that spin-dependent interactions between chiral molecules and magnetic surfaces can become more effective at higher temperatures, providing new insight into the microscopic origins of CISS and the environmental robustness of spin-controlled asymmetric processes.

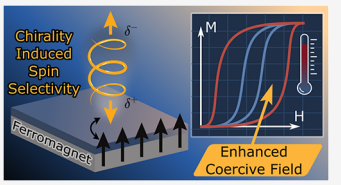

Downloaded via UPPSALA UNIV on June 9, 2026 at 08:13:17 (UTC).
See https://pubs.acs.org/sharingguidelines for options on how to legitimately share published articles.

The chiral-induced spin selectivity (CISS) effect is an empirical phenomenon revealing a strong interaction between electron spin and molecular chirality, even at room temperature.[1−3] The strong spin-chirality coupling due to CISS[4,5] allows for achiral magnetic minerals to function as chiral reagents for chemical reactions, which can be controlled by electron spin.[6−8] Concurrently, the reciprocal nature of this effect was demonstrated by showing that chiral molecules can induce magnetization on magnetic thin films[9−11] and locally change the magnetic anisotropy of thin films[12,13] (Figure 1a). Although various independent measurements confirm CISS-related effects, a complete microscopic understanding of CISS remains an ongoing challenge.[14] Notably, recent theoretical work by Fransson emphasizes the role of electron correlations in explaining the high levels of spin polarization observed in experiments.[15]

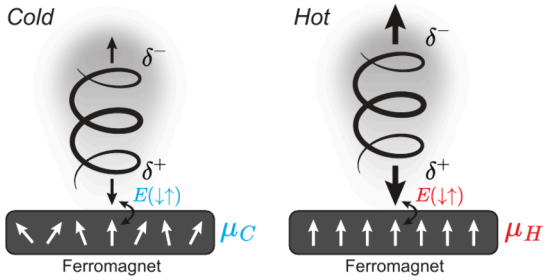

Figure 1. Chiral molecules can alter the magnetic properties of ferromagnetic surfaces through spin-exchange interactions, arising from transient spin splitting in a chiral potential due to the chiral-induced spin selectivity (CISS) effect. Spin polarization across a chiral molecule due to CISS is higher at higher temperatures, leading to an increase in chirality-induced magnetization and enhanced ferromagnetic order at higher temperatures: $\mu_H > \mu_C$.

Additionally, the effect of temperature on CISS through electron−phonon interactions presents an intriguing complexity,[3,16,17] with experimental results showing trends that appear incompatible with each other.[18−21] This complexity is partly due to the fact that temperature also affects the material and molecular properties involved, complicating efforts to isolate the CISS component of the observed effects. To address these challenges, we examined the temperature dependence of chirality-induced avalanche magnetization in chiral ribose-aminooxazoline (RAO) crystals on magnetic surfaces stable within our temperature range (Figure 1). RAO is a conglomerate-forming central RNA and DNA precursor of prebiotic relevance, characterized by high thermodynamic stability and a well-established crystal structure, and it exhibits strong spin-dependent interactions with magnetic surfaces.[22−26]

In contrast to classical expectations for spin-controlled processes, our experimental results and theoretical analysis show that the adsorption of chiral molecules leads to a significant increase in magnetic coercivity—via their spin-selective

Received: March 4, 2026
Revised: April 11, 2026
Accepted: April 13, 2026
Published: April 20, 2026

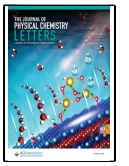

ACS Publications
© 2026 The Authors. Published by American Chemical Society

https://doi.org/10.1021/acs.jpclett.6c00705
J. Phys. Chem. Lett. 2026, 17, 5115−5121

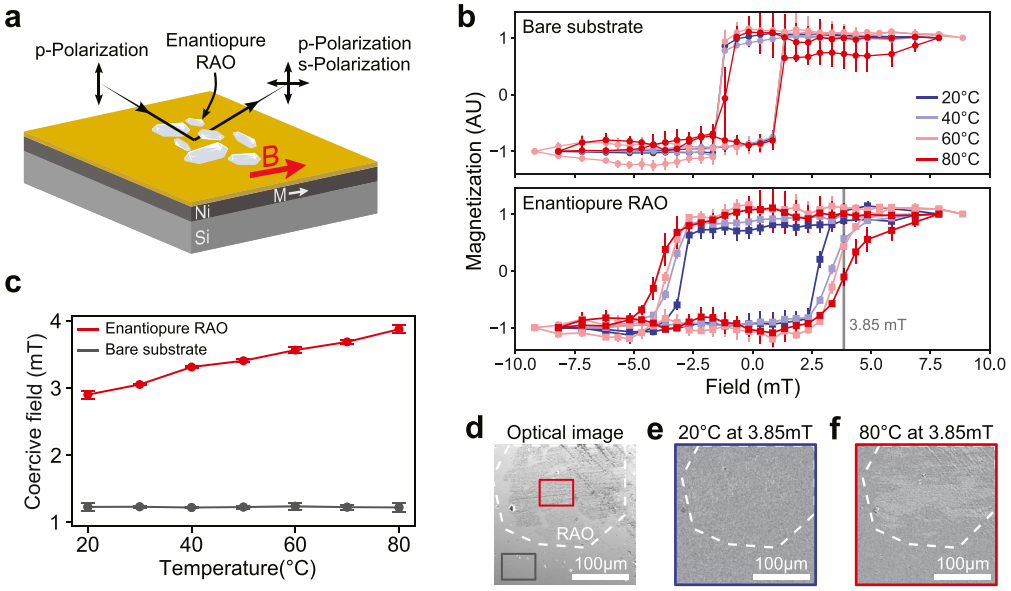

Figure 2. (a) Enantiopure RAO crystals were drop-cast onto a Si/Ni(50 nm)/Au(5 nm) thin film, forming a sample imaged with a MOKE microscope. In this setup, linearly polarized light is used to image the surface magnetization of the sample. The rotation of the polarization of the incident light corresponds to the surface magnetization. (b) Magnetic hysteresis loops are obtained by sweeping the magnetic field and averaging the intensity of regions far from (top) and beneath (bottom) homochiral L-RAO crystals. As the temperature increases, the loops beneath the crystals widen, indicating an increased coercive field, while the bare surface's coercive field remains constant. The vertical line at 3.85 mT is chosen to illustrate the difference in magnetization images at different temperatures, as seen in panels (e) and (f). (c) Coercive fields as a function of temperature for regions beneath (red) and far from (gray) the L-RAO crystals. The coercive field beneath the crystals is 2 mT higher at room temperature and increases linearly with rising temperature. (d) Optical image of the sample. A dashed white line outlines the area covered by L-RAO crystals, and regions beneath the crystals and far from the crystals, where magnetization loops were taken, are marked in red/gray, respectively. (e) Magnetic image at 20 °C and a 3.85 mT magnetic field, showing all domains flipped. (f) Magnetic image at 80 °C and a 3.85 mT magnetic field, where some domains beneath the crystals remain unflipped.

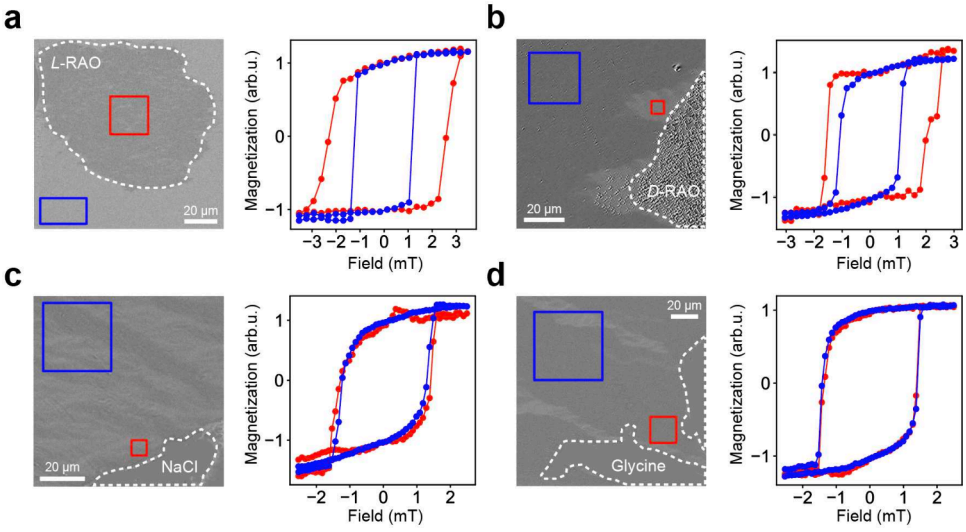

Figure 3. Kerr hysteresis loops of (a) L-RAO, (b) D-RAO, (c) glycine, and (d) NaCl on the Ni/Au substrate. Achiral crystals on the magnetic substrate do not lead to any change in the magnetic properties, whereas both enantiomers of RAO, a chiral crystal, lead to a significant increase in the coercive field. [Figure adapted from ref 9, Ozturk et al., "Chirality-induced avalanche magnetization of magnetite by an RNA precursor. *Nat. Commun.* *14*, 6351 (**2023**). Licensed under a Creative Commons Attribution 4.0 International License (http://creativecommons.org/licenses/by/4.0/)."]

interactions with the magnetic surface—that becomes more enhanced at higher temperatures (Figure 2). This supports a vibronic contribution to CISS, indicating that phonon-assisted couplings play a significant role in enhancing the ferromagnetic order due to the CISS effect.[27] These findings shed light on the temperature dependence of CISS, which remains an active area of research with seemingly incompatible findings.

We studied the effect of temperature on chirality-induced magnetization using a magneto-optical Kerr effect (MOKE) microscope and showed an increase in magnetic coercivity with increasing temperature.

MOKE microscopy is an optical technique used to measure the surface magnetization of a material by reflecting polarized light from its surface, producing image contrast that is directly proportional to the relative magnetization.[9,10,28] MOKE

https://doi.org/10.1021/acs.jpclett.6c00705
J. Phys. Chem. Lett. 2026, 17, 5115−5121

microscopy was used to measure the chirality-induced avalanche magnetization on a ferromagnetic surface by enantiopure RAO crystals.

Enantiopure RAO crystals were formed on a Si/Ni(50 nm)/Au(5 nm) thin film by drop-casting an RAO water solution, as illustrated in Figure 2a. A commercial Evico-Magnetics GmbH Magneto-optical Kerr effect (MOKE) microscope, equipped with an electromagnet oriented parallel to the sample surface, was used to image the local magnetic effects induced by the enantiopure RAO crystals. The MOKE microscope provides qualitative imaging of surface magnetization by detecting the Kerr rotation, which reflects the change in the linear polarization of light as a function of the local magnetization (Figure 2a). The contrast in the MOKE images corresponds to regions with different magnetization directions relative to the incident light, allowing us to assess the influence of the enantiopure RAO crystals on adjacent magnetic domains. It is important to note that MOKE microscopy here is not used for measuring induced magnetization upon adsorption of RAO molecules, but the coercive field of the sample with and without the RAO molecules, i.e., the sample's response to an outer magnetic field.

Surface magnetization images of the Ni film around the enantiopure RAO crystals at different magnetic fields and temperatures (20 °C, blue; 40 °C, light blue; 60 °C, light red; 80 °C, red) were taken. Magnetic hysteresis loops were obtained from surface magnetization images by sweeping the magnetic field and averaging the intensity in areas far (Figure 2b, top) and under (Figure 2b, bottom) from the enantiopure RAO crystals within the same image. In the demagnetized state (presented in Figure S7), the crystals appear to partially destroy the alignment of the magnetic domains but do not affect the domain size. As the temperature increases, the magnetic hysteresis loops under the crystals widen, indicating an increase in the coercive field. In contrast, the coercive field of the bare magnetic surface far from the crystals remains constant across all temperatures. During the measurements, RAO crystals remain stable at all temperatures. Racemic RAO was not studied since RAO crystallizes as a conglomerate, inevitably creating homochiral domains. Achiral crystals of glycine and sodium chloride were studied under the same conditions as control experiments (Figure 3). Unlike the chiral samples, they showed no change in coercivity relative to the bare substrate. Taken together, the Au spacer layer, the absence of a comparable response for achiral control crystals, further confirm that the observed effect arises from molecular chirality and argue against a purely trivial surface modification or roughness-based origin of the effect. Moreover, conventional pinning- or roughness-based coercivity mechanisms do not naturally account for the observed RAO-specific enhancement with increasing temperature.[29]

Starting with a negative field that saturates the sample, a uniform dark magnetization is observed, corresponding to −1 magnetization. As the magnetic field increases, the Ni magnetization flips to bright (+1 magnetization) at 1 mT; however, it requires an additional 2 mT to flip the domains surrounding the RAO crystals. When sweeping the field back down, the domains far from the crystals flip at −1 mT, while those under the crystals flip at −3 mT. A video of the MOKE images during a single sweep is presented in Videos S1 and S2, and an example of the resulting images is presented in Figure S3. The coercive field is plotted as a function of temperature in Figure 2c for regions under (red) and far (gray) from the crystals. The coercive field under the crystal is 2 mT higher than that of the bare surface far from the crystals and increases linearly with temperature.

The optical image of the sample is shown in Figure 2d with the area of the crystals marked in a dashed white line. The areas under the crystals (red) or far from the crystals (gray) from which the magnetization loops were taken are marked on the image. Corresponding magnetic images at a magnetic field of 3.85 mT are shown in Figure 2e (20 °C) and Figure 2f (80 °C). In this field, all the domains flipped at 20 °C, while at 80 °C, some light domains are left under the crystals. Both enantiomers of RAO were studied, and they led to similar phenomena of increased magnetic coercivity, as presented in Section S1.2 in the Supporting Information.

At higher temperatures, a more gradual transition from one magnetization to the other under the crystals is seen by the increasingly slow transition toward magnetic saturation in the magnetic hysteresis loops in Figure 2b. This behavior likely arises from reduced domain size at higher temperatures. Consequently, although the coercive field is stronger, the extent of avalanche magnetization decreases (Section S1.5 in the Supporting Information), highlighting a tradeoff between the strength of induced magnetization and its spatial spread with increasing temperatures.

How can we account for the increased effectiveness of CISS with temperature without involving microscopic details? We will start with an intuitive thermodynamic picture and incorporate microscopic analyses later in the discussion.

CISS relates to the spin-filtering of electrons, meaning that chiral molecules reduce entropy by decreasing the number of accessible microstates of the electronic spin distribution at the molecule−surface interface.

We first consider the electronic spin distribution as the system of interest. To leading order, electron number and energy are conserved during spin filtering, allowing this subsystem to be described within a microcanonical ensemble. According to the first law of thermodynamics,

$$\mathrm{d}E = T\,\mathrm{d}S + \mathrm{d}W = 0$$

Spin filtering reduces the number of accessible spin microstates, implying $\mathrm{d}S < 0$ for the electronic subsystem. This entropy reduction requires positive work to be performed by the chiral molecules.

We next consider the chiral molecules as a separate subsystem interacting with their surroundings. Since the entropy of the electronic subsystem decreases, the entropy of the chiral molecules must increase according to the second law of thermodynamics. The free energy change of the molecular subsystem is

$$\mathrm{d}G = \mathrm{d}H - T\mathrm{d}S$$

Because $\mathrm{d}S > 0$ for the molecules, the $-T\,\mathrm{d}S$ term becomes increasingly negative at higher temperatures. Since the spin filtering process is not spontaneous, heat must be supplied to the molecular subsystem to maintain a positive free-energy cost.

In this picture, chiral molecules operate by absorbing heat from their surroundings and converting it into work that reduces the entropy of the electronic spin distribution. Consequently, chiral molecules operate more effectively when heat is provided.

This thermodynamic picture is an intuitive way of visualizing the temperature dependence of CISS. However, the effect itself is a complex phenomenon involving spin−orbit coupling, electron correlations, and electron spin-phonon interactions. Fransson investigated the role of phonons and vibronic

https://doi.org/10.1021/acs.jpclett.6c00705
J. Phys. Chem. Lett. 2026, 17, 5115−5121

interactions in CISS, constructing a microscopic theory of CISS beyond the Born−Oppenheimer approximation. This model elucidates the exchange of angular momentum as electrons traverse a helical trajectory,[17,30] which is introduced below and elaborated upon in our complementary theoretical study.[27] Our experimental results align with this microscopic framework, indicating that phonon-chirality couplings, amplified by temperature, play an essential role in CISS.

Having provided an intuitive thermodynamic picture, we will now present a microscopic model connecting phonons to electron spin, and thereby to magnetization. In this sense, the two descriptions are complementary: the above-mentioned framework provides the thermodynamic interpretation, while Figure Figure 4 presents its microscopic realization.

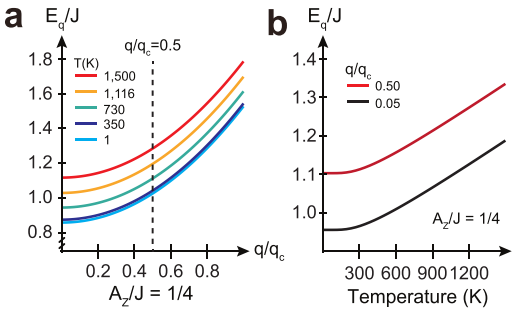

Figure 4. Magnon energy dispersion relation as a function of (a) coupling strength between spin and vibrational modes, q, for five different temperatures between 1 K and 1500 K and (b) temperature for two different values of q. Here, the spin−lattice coupling $A_z = 1/4$, axial anisotropy $I_0 = -1/8$ in units of $J = 80$ meV.

The strength of the coercive field is a measure of the axial magnetic anisotropy, which corresponds to the energy barrier stabilizing a ferromagnet against spin excitations. These spin excitations, or magnons, are essentially destructive to the ferromagnetic order. However, by studying the magnon spectrum, we gain insight into the cause of the temperature-enhanced coercive field observed in the experiments (Figure 2).

The anisotropic Heisenberg model describes the magnetic excitations for a collection of interacting spin moments S_i distributed on a two-dimensional lattice at the coordinates r_i. In Hamiltonian form, this model can be written as

$$H_H = -J \sum_{ij} \mathbf{S}_i \cdot \mathbf{S}_j - I \sum_{ij} S_i^z S_j^z \tag{1}$$

where the first term accounts for isotropic interactions between the spins, while the second provides an axial anisotropy, resulting in a preferred orientation for the total magnetic moment. The interaction parameters J and I are chosen to be positive, such that a ferromagnetic ground state is favored.

This model is capable of describing the ferromagnetic state of a local moment ferromagnet for temperatures below the Curie temperature, T_C. While the Heisenberg interaction J defines a ferromagnetic ground state, this state is spatially isotropic, with the effect that a magnetic moment cannot be derived solely in terms of this interaction. This is also a consequence of the Mermin and Wagner theorem, which states that local isotropic interactions cannot give rise to long-range order for systems with spatial dimensions less than three.[31] The anisotropic contribution I relaxes this fundamental principle and introduces an energy gap such that any excited state of the spin system requires additional energy to be occupied—energy that may be provided by the temperature of the surrounding environment. Eventually, this energy gap is closed by the thermal energy at sufficiently high temperatures, leading to the destruction of the ferromagnetic order. This is the reason for the destruction of ferromagnetism with temperature.

The unexpected increase in magnetic coercivity with temperature observed in this work can be explained by the coupling between nuclear vibrations and the localized spin moment.[32] This is the origin of the enhanced chirality-induced magnetization with increasing temperatures.

This interaction is captured by the addition of

$$H_{SQ} = -\sum_{ij} \mathbf{S}_i \cdot \mathbb{A}_{ij} \cdot \mathbf{Q}_j \tag{2}$$

where Q_i denotes the spatial displacement of the nucleus at r_i, while $\mathbb{A}_{ij}$ represents a coupling between the localized spin moment at S_i and the displacement Q_j (or the nucleus at r_j). The nuclear displacements result in a field acting on the localized spin moments, resembling that of a magnetic field; hence, we may refer to it as a pseudomagnetic field. It should be noted that $\mathbb{A}_{ij}$ is a tensorial interaction with the form of a susceptibility, which arises from charge-spin fluctuations in the compound. While this susceptibility can be considered negligible in inversion-symmetric crystal structures, $\mathbb{A}_{ij}$ is nonvanishing in chiral structures,[33] where inversion symmetry is broken by definition. Introducing this component to the model is relevant in the current context, where we have chiral molecules adsorbed on a magnetite surface.

As we are interested in the effect of the spin−lattice coupling on the magnetic anisotropy, we consider the linear spin wave spectrum that results from the introduced model. The details are presented in a complementary work,[27] and here, we merely present the salient features from this investigation.

In the absence of spin−lattice coupling, at lower temperatures, the linear spin wave spectrum in the limit of long wavelength is captured by the energy dispersion relation $E_q = \alpha q^2 + \beta$, where q is the reciprocal of the wavelength, $\alpha > 0$ is related to the exchange energy J, and $\beta > 0$ represents the anisotropic energy in terms of I. Therefore, the physics of the composed system is dominated by processes that are very well captured within this theoretical picture.

At higher temperatures, the dominant processes that govern the physics are related to the spin−lattice coupling, such that the energy dispersion relation must be replaced by $E_q(T) = \alpha q^2 + \beta + \gamma T$, where the additional anisotropic contribution γ provides a linear temperature dependence of the energy dispersion, as seen in the plotted curve in Figure 4. The derivation of this linearity is discussed in ref 27 and in section S4 in the SI. The effect of this linear contribution to the anisotropy energy leads to an increase in the coercive field with temperature, in agreement with the experimental observations (Figure 2). We do not assign specific RAO phonon modes in the present work. Rather, we interpret the temperature-dependent term phenomenologically as reflecting coupling to low-energy chiral vibrational degrees of freedom, which are expected to be the most relevant modes for angular momentum exchange,where the coupling is enhanced by increasing temperatures, in localized molecular systems.[34] Raman data for RAO are provided in the Supporting Information (Figure S13), while a direct next step will be to combine such characterization with VCD to identify and selectively test chiral low-energy modes. Physically, we interpret this addition to the anisotropic energy as a new channel that

https://doi.org/10.1021/acs.jpclett.6c00705
J. Phys. Chem. Lett. 2026, 17, 5115−5121

diverts the energy away from spin excitations of the system through spin−lattice coupling. This term is connected to the heat supplied to the chiral molecules, as we explained in the thermodynamic picture.

The combination of these two terms—one being destructive and the other constructive to the thermodynamic order—stabilizes the system of chiral molecules on a magnetic surface against thermal fluctuations. This provides the persistent magnetization required to observe spin-controlled asymmetric processes arising from CISS in natural environments. This inherent stability of our mechanism, together with RAO's superior thermodynamic stability,[35] enhances our scenario's environmental plausibility.

The magnetic response in our system manifests primarily as an increase in coercive field, rather than as a reversal of the net magnetization. This behavior differs from earlier reports of magnetization switching in perpendicular-anisotropy stacks,[11] which are distinct from both our in-plane Ni/Au films and bulk magnetite.

The MOKE loops remain symmetric in our measurements and show no evidence of exchange bias, although we cannot fully exclude subtle effects below our detection threshold. This observation supports a scenario of anisotropy change rather than molecule-driven magnetization switching. A possible explanation is that the molecules induce local magnetic moments at the surface.[36] Such surface effects can alter magnetic anisotropy but may not be sufficient to reverse the magnetization of the ferromagnet within an exchange length.

To distinguish between coercivity enhancement and true magnetization switching, we performed complementary Hall effect measurements on Ni films with Au or oxide capping layers (Section S2 in the Supporting Information). These measurements show an increase in Hall resistance upon RAO adsorption; however, the response lacks consistent directionality, likely due to nonspecific molecular binding at the surface. Therefore, based on our current measurements, we cannot conclude that RAO induces net magnetization switching in Ni/Au systems. However, our theoretical model allows us to probe the net magnetization induced by chiral molecules and its temperature dependence. It predicts that M_z, the net out-of-plane magnetization, decreases with increasing temperature,[27] unlike the magnetic coercivity, which is enhanced with temperature in agreement with our measurements.

Surface chemistry appears central to these considerations. On magnetite, the magnetic surface that was studied in connection to prebiotic chemistry of RAO, RAO directly binds through hydrogen bonding, a strong chemical interaction that brings the molecules into close proximity with the substrate. In contrast, on 5-nm gold-capped nickel, RAO interacts more weakly and less directly through electrostatic forces. This weaker physisorption also keeps the molecules farther from the surface, leading to reduced interfacial coupling and less-organized dipole orientation. Molecular orientation is particularly important: as shown by Nguyen et al.,[37] oppositely oriented molecules can invert the direction of the CISS effect, and strong collective coalignment of molecules is required for a strong CISS signal. Unlike more orientation-controlled CISS platforms, the drop-cast RAO crystals in the present Ni/Au geometry do not provide independent control over the molecular/crystallographic orientation relative to the surface or to the in-plane applied field. Consistent with Hall measurements showing no magnetization reversal, the present MOKE measurements probe a chirality-induced change in coercivity under heterogeneous interfacial orientations.

Nickel surfaces introduce an additional complication. Their metallic nature induces a mirror potential that screens surface charges, effectively reducing the influence of adsorbed molecules on spin-dependent charge redistribution due to CISS.[38] This screening effect should be weaker on semiconducting magnetite, allowing stronger proximity interactions with chiral molecules.

In summary, RAO adsorption on magnetite produces a more pronounced CISS effect than on Ni/Au. This enhancement arises from (i) stronger chemical binding, (ii) stronger alignment of dipoles, (iii) closer molecular proximity to the surface, and (iv) weaker electronic screening by the semiconducting substrate.

Our earlier studies of RAO on magnetite, which revealed a handedness-dependent inversion of the circular dichroism signal, suggest that the RAO−magnetite interface can produce a net magnetization change within the magnetite exchange length (around 9 nm). In contrast, MOKE measurements of RAO on Ni/Au show no evidence of exchange bias in the hysteresis loops.[9] Taken together, these results clarify the subtle differences in the magnetic behavior of RAO on magnetite versus Ni/Au and provide a mechanistic basis for the enhanced CISS effect observed on magnetite.

Last but not least, it is important to consider the magnetic configuration of the film. Our MOKE measurements show that the observed response is strongly shaped by the fact that the present system is an in-plane, multidomain thin film. In such films, full in-plane magnetization reversal within the material's exchange length requires a strong induced effective magnetic field, whereas coercivity can increase more readily through local changes in anisotropy. Under these conditions, any induced magnetization is transient and disappears once the molecules are removed. In contrast, systems with frustrated geometries—such as perpendicular-anisotropy stacks or single-domain particles—are more susceptible to stable magnetization reversal. Single-domain, low-coercivity magnetite particles represent the most suitable magnetic substrates for our system. It is therefore important to investigate whether RAO can induce permanent magnetization switching in these low-coercivity grains. These particles are also geochemically plausible under early Earth and Martian conditions and can be synthesized prebiotically from iron−carbonate solutions.[39,40]

Our findings show that spin-controlled asymmetric processes due to the CISS effect can locally increase the coercivity of a ferromagnetic thin film. Contrary to classical expectations, temperature, which is an important environmental variable, actually enhances this process. Our experiments reveal that chirality-induced coercivity by RAO becomes stronger as the temperature increases. These results not only provide insights into the temperature dependence of CISS, an active area of research, but also reinforce the stability of spin-controlled mechanisms involving CISS across various environmental conditions. The inherent stability of CISS, which distinguishes it from classical magnetic phenomena, arises from spin-phonon couplings, which appear to be crucial for the high degree of spin polarization observed in CISS experiments. Thus, our results offer both a deeper understanding of CISS and highlight its significance in the context of the origin of life's homochirality.

https://doi.org/10.1021/acs.jpclett.6c00705
J. Phys. Chem. Lett. 2026, 17, 5115−5121

EXPERIMENTAL SECTION

Preparation of Magnetic Surfaces

For the MOKE measurements, ferromagnetic Ti (8 nm)/Ni (30 nm)/Au (5 nm) surfaces were evaporated by electron beam under a high-vacuum of 3×10^{-7} Torr on silicon (100) wafer. The thin gold coating was used to prevent the oxidation of the magnetic substrate and preserve its spin-polarization properties. The surfaces were cleaned thoroughly with acetone and ethanol before every experiment.

For the Hall measurements, Ni (40 nm)/Au (10 nm) surfaces were evaporated onto a Si/SiO wafer using electron beam evaporation (VST Metals Evaporator) under pressure of 3×10^{-6} Torr. An aluminum mask was used to form four, 3 mm × 3 mm,[2] corner contact pads on the sample for better electrical connectivity to the surface. Ti(10 nm)/Au(50 nm) pads were evaporated under cooling conditions on top of the surface.

RAO Synthesis

D- and L-ribo-aminooxazolines (RAO) were synthesized by the reaction of 2 equiv of cyanamide (5 g, 0.12 mol) with 1 equiv of the D- and D-ribose (9 g, 0.06 mol) in aqueous ammonia (3.5%, 10 mL). After the reaction, enantiopure RAO was crystallized, the solution was filtered, and the crystals were dried and ground into powder. Twenty (20) mM solutions of D- or L-RAO were prepared in pure water and used in the experiments.

RAO Crystallization

For the MOKE experiments, small (around 1−10 μm) and dense crystals were obtained by drop casting 5 μL of L/D-RAO solution on Ti (8 nm)/Ni (30 nm)/Au (5 nm) surfaces. Samples were then placed in the fridge (−18 °C) for two cycles of 2 h, with a 2 h interval at room temperature. Finally, samples were dried overnight at room temperature and areas of amorphous aggregation and dense crystallization were obtained. For the hall experiments, 10 μL D-RAO solution was drop-cast onto the Ni(40 nm)/Au(10 nm) surface and dried overnight at room temperature.

MOKE Microscopy

MOKE imaging and magnetometry were performed using a commercial Evico Magnetics GmbH magnetooptical Kerr microscope. The measurements were taken in the longitudinal configuration. An in-plane magnetic field was generated by an electromagnet obtained from the microscope supplier powered by a Kepco BOP 100−4DL power supply. For the optical imaging of substrates, 20× commercial Zeiss objective lenses were used. A piezo stage actively stabilized mechanical vibrations of the sample. Temperature was controlled by a Peltier element and was measured continuously using a Pt thermistor.

ASSOCIATED CONTENT

Supporting Information

The Supporting Information is available free of charge at https://pubs.acs.org/doi/10.1021/acs.jpclett.6c00705.

Figures S1−13: Additional MOKE data for both RAO enantiomers; analysis of temperature-dependent domain behavior and avalanche magnetization; Hall effect measurements on Ni films with Au and oxide capping layers; derivation of the linear temperature-dependent term used in the microscopic model (PDF)

AUTHOR INFORMATION

Corresponding Author

S. Furkan Ozturk − *Division of Geological and Planetary Sciences, California Institute of Technology, Pasadena, California 91125, United States;* orcid.org/0000-0003-1830-3619; Email: ozturk@caltech.edu

Authors

Yael Kapon − *Department of Applied Physics, The Hebrew University, Jerusalem 9190401, Israel;* orcid.org/0000-0001-5019-2117

Lilach Brann − *Department of Applied Physics, The Hebrew University, Jerusalem 9190401, Israel*

Shira Yochelis − *Department of Applied Physics, The Hebrew University, Jerusalem 9190401, Israel;* orcid.org/0000-0001-9180-4669

Jonas Fransson − *Department of Physics and Astronomy, Uppsala University, Uppsala 752 37, Sweden;* orcid.org/0000-0002-9217-2218

Dimitar D. Sasselov − *Department of Astronomy, Harvard University, Cambridge, Massachusetts 02138, United States*

Yossi Paltiel − *Department of Applied Physics, The Hebrew University, Jerusalem 9190401, Israel;* orcid.org/0000-0002-8739-9952

Complete contact information is available at: https://pubs.acs.org/10.1021/acs.jpclett.6c00705

Author Contributions

‖Authors Y. Kapon and L. Brann contributed equally to this work.

Notes

The authors declare no competing financial interest.

ACKNOWLEDGMENTS

We thank Dr. Anastasia Yanchilina from California Institute of Technology for her assistance with Raman measurements. We thank Naama Goren from the Hebrew University Applied Physics Department for her help in interpreting the Hall measurements and Maurice Saidian and Alexander Oginets from the Hebrew University Nano Center for Ni/Au evaporation. Y.P. acknowledges the funding from Marie Skłodowska-Curie Actions under Horizon Europe framework program (CISSE Project No. 101071886), Carl Zeiss Stiftung (HYMMS Project No. P2022-03-044), and U.S Air Force (Grant No. FA8655-24-1-7390). Y.K. thanks the Israel Council of Higher Education's VTT fellowship for women in STEM. S.F.O. and D.D.S. acknowledge the Harvard Origins of Life Initiative for funding and its members for fruitful discussions. S.F.O. further acknowledges support from the Kavli-Laukien fellowship program, Caltech startup funds, the William H. Hurt Scholarship Program, and the Fellows of King's College Cambridge for their hospitality. J.F. acknowledges support from Olle Engkvists Stiftelse.

REFERENCES

(1) Naaman, R.; Waldeck, D. H. Chiral-induced spin selectivity effect. *J. Phys. Chem. Lett.* **2012**, *3*, 2178−2187.

(2) Naaman, R.; Paltiel, Y.; Waldeck, D. H. Chiral molecules and the electron spin. *Nat. Rev. Chem.* **2019**, *3*, 250−260.

(3) Bloom, B. P.; Paltiel, Y.; Naaman, R.; Waldeck, D. H. Chiral Induced Spin Selectivity. *Chem. Rev.* **2024**, *124*, 1950.

(4) Ziv, A.; Saha, A.; Alpern, H.; Sukenik, N.; Baczewski, L. T.; Yochelis, S.; Reches, M.; Paltiel, Y. AFM-Based Spin-Exchange Microscopy Using Chiral Molecules. *Adv. Mater.* **2019**, *31*, 1904206.

(5) Safari, M. R.; Matthes, F.; Caciuc, V.; Atodiresei, N.; Schneider, C. M.; Ernst, K.-H.; Bürgler, D. E. Enantioselective adsorption on magnetic surfaces. *Adv. Mater.* **2024**, *36*, 2308666.

(6) Banerjee-Ghosh, K.; Ben Dor, O.; Tassinari, F.; Capua, E.; Yochelis, S.; Capua, A.; Yang, S.-H.; Parkin, S. S. P.; Sarkar, S.; Kronik, L.; Baczewski, L. T.; Naaman, R.; Paltiel, Y. Separation of enantiomers

by their enantiospecific interaction with achiral magnetic substrates. *Science* **2018**, *360*, 1331−1334.
(7) Bloom, B.; Lu, Y.; Metzger, T.; Yochelis, S.; Paltiel, Y.; Fontanesi, C.; Mishra, S.; Tassinari, F.; Naaman, R.; Waldeck, D. Asymmetric reactions induced by electron spin polarization. *Phys. Chem. Chem. Phys.* **2020**, *22*, 21570−21582.
(8) Metzger, T. S.; Siam, R.; Kolodny, Y.; Goren, N.; Sukenik, N.; Yochelis, S.; Abu-Reziq, R.; Avnir, D.; Paltiel, Y. Dynamic Spin-Controlled Enantioselective Catalytic Chiral Reactions. *J. Phys. Chem. Lett.* **2021**, *12*, 5469−5472.
(9) Ozturk, S. F.; Bhowmick, D. K.; Kapon, Y.; Sang, Y.; Kumar, A.; Paltiel, Y.; Naaman, R.; Sasselov, D. D. Chirality-induced avalanche magnetization of magnetite by an RNA precursor. *Nat. Commun.* **2023**, *14*, 6351.
(10) Kapon, Y.; Kammerbauer, F.; Yochelis, S.; Kläui, M.; Paltiel, Y. Magneto-optical imaging of magnetic-domain pinning induced by chiral molecules. *J. Chem. Phys.* **2023**, *159*, DOI: 10.1063/5.0159351.
(11) Ben Dor, O.; Yochelis, S.; Radko, A.; Vankayala, K.; Capua, E.; Capua, A.; Yang, S.-H.; Baczewski, L. T.; Parkin, S. S. P.; Naaman, R.; Paltiel, Y. Magnetization switching in ferromagnets by adsorbed chiral molecules without current or external magnetic field. *Nat. Commun.* **2017**, *8*, 1−7.
(12) Sun, R.; Wang, Z.; Bloom, B. P.; Comstock, A. H.; Yang, C.; McConnell, A.; Clever, C.; Molitoris, M.; Lamont, D.; Cheng, Z.-H.; et al. Colossal anisotropic absorption of spin currents induced by chirality. *Sci. Adv.* **2024**, *10*, No. eadn3240.
(13) Moharana, A.; Kapon, Y.; Kammerbauer, F.; Anthofer, D.; Yochelis, S.; Shema, H.; Gross, E.; Kläui, M.; Paltiel, Y.; Wittmann, A. Chiral-induced unidirectional spin-to-charge conversion. *Sci. Adv.* **2025**, *11*, No. eado4285.
(14) Evers, F.; Aharony, A.; Bar-Gill, N.; Entin-Wohlman, O.; Hedegård, P.; Hod, O.; Jelinek, P.; Kamieniarz, G.; Lemeshko, M.; Michaeli, K.; et al. Theory of chirality induced spin selectivity: Progress and challenges. *Adv. Mater.* **2022**, *34*, 2106629.
(15) Fransson, J. Chirality-induced spin selectivity: The role of electron correlations. *J. Phys. Chem. Lett.* **2019**, *10*, 7126−7132.
(16) Kim, K.; Vetter, E.; Yan, L.; Yang, C.; Wang, Z.; Sun, R.; Yang, Y.; Comstock, A. H.; Li, X.; Zhou, J.; Zhang, L.; You, W.; Sun, D.; Liu, J. Chiral-phonon-activated spin Seebeck effect. *Nat. Mater.* **2023**, *22*, 322−328.
(17) Fransson, J. Vibrational origin of exchange splitting and chiral-induced spin selectivity. *Phys. Rev. B* **2020**, *102*, 235416.
(18) Das, T. K.; Tassinari, F.; Naaman, R.; Fransson, J. Temperature-dependent chiral-induced spin selectivity effect: Experiments and theory. *J. Phys. Chem. C* **2022**, *126*, 3257−3264.
(19) Qian, Q.; Ren, H.; Zhou, J.; Wan, Z.; Zhou, J.; Yan, X.; Cai, J.; Wang, P.; Li, B.; Sofer, Z.; Li, B.; Duan, X.; Pan, X.; Huang, Y.; Duan, X. Chiral molecular intercalation superlattices. *Nature* **2022**, *606*, 902−908.
(20) Alwan, S.; Sarkar, S.; Sharoni, A.; Dubi, Y. Temperature-dependence of the chirality-induced spin selectivity effect—Experiments and theory. *J. Chem. Phys.* **2023**, *159*. DOI: 10.1063/5.0147886
(21) Yang, C.; Li, Y.; Zhou, S.; Guo, Y.; Jia, C.; Liu, Z.; Houk, K. N.; Dubi, Y.; Guo, X. Real-time monitoring of reaction stereochemistry through single-molecule observations of chirality-induced spin selectivity. *Nat. Chem.* **2023**, *15*, 972−979.
(22) Springsteen, G.; Joyce, G. F. Selective derivatization and sequestration of ribose from a prebiotic mix. *J. Am. Chem. Soc.* **2004**, *126*, 9578−9583.
(23) Patel, B. H.; Percivalle, C.; Ritson, D. J.; Duffy, C. D.; Sutherland, J. D. Common origins of RNA, protein and lipid precursors in a cyanosulfidic protometabolism. *Nature Chem.* **2015**, *7*, 301−307.
(24) Powner, M. W.; Gerland, B.; Sutherland, J. D. Synthesis of activated pyrimidine ribonucleotides in prebiotically plausible conditions. *Nature* **2009**, *459*, 239−242.
(25) Xu, J.; Chmela, V.; Green, N. J.; Russell, D. A.; Janicki, M. J.; Góra, R. W.; Szabla, R.; Bond, A. D.; Sutherland, J. D. Selective prebiotic formation of RNA pyrimidine and DNA purine nucleosides. *Nature* **2020**, *582*, 60−66.
(26) Ozturk, S. F.; Liu, Z.; Sutherland, J. D.; Sasselov, D. D. Origin of biological homochirality by crystallization of an RNA precursor on a magnetic surface. *Sci. Adv.* **2023**, *9*, No. eadg8274.
(27) Fransson, J.; Kapon, Y.; Brann, L.; Yochelis, S.; Sasselov, D. D.; Paltiel, Y.; Ozturk, S. F. Chiral Phonons Enhance Ferromagnetism. *J. Phys. Chem. Lett.* **2025**, *16*, 2001−2007.
(28) Sharma, A.; Matthes, P.; Soldatov, I.; Arekapudi, S. S. P. K.; Bohm, B.; Lindner, M.; Selyshchev, O.; Thi Ngoc Ha, N.; Mehring, M.; Tegenkamp, C.; et al. Control of magneto-optical properties of cobalt-layers by adsorption of α-helical polyalanine self-assembled monolayers. *J. Mater. Chem. C* **2020**, *8*, 11822−11829.
(29) Kronmüller, H. Theory of the coercive field in amorphous ferromagnetic alloys. *J. Magn. Magn. Mater.* **1981**, *24*, 159−167.
(30) Fransson, J. Charge and spin dynamics and enantioselectivity in chiral molecules. *J. Phys. Chem. Lett.* **2022**, *13*, 808−814.
(31) Mermin, N. D.; Wagner, H. Absence of ferromagnetism or antiferromagnetism in one-or two-dimensional isotropic Heisenberg models. *Phys. Rev. Lett.* **1966**, *17*, 1133.
(32) Fransson, J.; Thonig, D.; Bessarab, P. F.; Bhattacharjee, S.; Hellsvik, J.; Nordström, L. Microscopic theory for coupled atomistic magnetization and lattice dynamics. *Physical review materials* **2017**, *1*, 074404.
(33) Fransson, J. Chiral phonon induced spin polarization. *Phys. Rev. Res.* **2023**, *5*, L022039.
(34) Naaman, R.; Paltiel, Y. Why Is the Mechanism Underlying the Chiral-Induced Selectivity Effect Still Challenging? *Adv. Mater.* **2026**, No. e23675.
(35) Powner, M. W.; Sutherland, J. D. Phosphate-mediated interconversion of ribo-and arabino-configured prebiotic nucleotide intermediates. *Angew. Chem., Int. Ed.* **2010**, *49*, 4641−4643.
(36) Alwan, S.; Dubi, Y. Spinterface origin for the chirality-induced spin-selectivity effect. *J. Am. Chem. Soc.* **2021**, *143*, 14235−14241.
(37) Nguyen, T. N. H.; Salvan, G.; Hellwig, O.; Paltiel, Y.; Baczewski, L. T.; Tegenkamp, C. The mechanism of the molecular CISS effect in chiral nano-junctions. *Chemical Science* **2024**, *15*, 14905−14912.
(38) Liu, P.-Y.; Zhang, T.-Y.; Sun, Q.-F. Dynamical Simulation of Chiral-Induced Spin-Polarization and Magnetization. *J. Phys. Chem. Lett.* **2025**, *16*, 6500−6506.
(39) Hurowitz, J. A.; Grotzinger, J. P.; Fischer, W. W.; McLennan, S. M.; Milliken, R. E.; Stein, N.; Vasavada, A. R.; Blake, D. F.; Dehouck, E.; Eigenbrode, J. L.; et al. Redox stratification of an ancient lake in Gale crater, Mars. *Science* **2017**, *356*, No. eaah6849.
(40) Tosca, N.; Ahmed, I.; Tutolo, B.; Ashpitel, A.; Hurowitz, J. Magnetite Authigenesis and the Warming of Early Mars. *Nature Geoscience* **2018**, *11*, 635−639.

https://doi.org/10.1021/acs.jpclett.6c00705
J. Phys. Chem. Lett. 2026, 17, 5115−5121